Earth, Planets and Space

FULL PAPER

Open Access

On the characterization of tidal ocean-dynamo signals in coastal magnetic observatories

Johannes Petereit[1,2*], Jan Saynisch-Wagner[1], Achim Morschhauser[1], Leonie Pick[3] and Maik Thomas[1,2]

Abstract

Periodic tidal ocean currents induce electric currents and, therefore, magnetic field signals that are observable using spaceborne and ground-based observation techniques. In theory, the signals can be used to monitor oceanic temperature and salinity variations. Tidal magnetic field amplitudes and phases have been extracted from magnetometer measurements in the past. However, due to uncertainties caused by a plentitude of influencing factors, the shape and temporal variation of these signals are only known to a limited extent. This study uses past extraction methods to characterize seasonal variations and long-term trends in the ten year magnetometer time series of three coastal island observatories. First, we assess data processing procedures used to prepare ground-based magnetometer observations for tidal ocean dynamo signal extraction to demonstrate that existing approaches, i.e., subtraction of core field models or first-order differencing, are unable to reliably remove low-frequency contributions. We hence propose low-frequency filtering using smoothing splines and demonstrate the advantages over the existing approaches. Second, we determine signal and side peak magnitudes of the M2 tide induced magnetic field signal by spectral analysis of the processed data. We find evidence for seasonal magnetic field signal variations of up to 25% from the annual mean. Third, to characterize the long-term behavior of tidal ocean dynamo signal amplitudes and phases, we apply different signal extraction techniques to identify tidal ocean-dynamo signal amplitudes and phases in sub-series of the ten-year time series with incrementally increasing lengths. The analyses support three main findings: (1) trends cause signal amplitude changes of up to $\approx$ 1nT and phase changes are in the order of $\mathcal{O}(10°)$ within the observation period; (2) at least four years of data are needed to obtain reliable amplitude and phase values with the extraction methods used and (3) signal phases are a less dependent on the chosen extraction method than signal amplitudes.

Keywords: Ocean-tide induced magnetic fields, Tidal ocean dynamo, EMOTS, Signal extraction, Magnetometer Observations, Data Processing

Introduction

Motional induction describes the generation of electric currents through the movement of charge carriers within an ambient magnetic field. It is the working principle of a dynamo or generator and also generates electric currents in the ocean. There, electrically charged particles (salt ions) move relative to an ambient magnetic field (the geomagnetic field). In contrast to a generator, where the Lorentz force acts on the free electrons within the metal conductor and creates thus a current, the electric current in the ocean is generated when positive and negative salt ions are deflected in opposing directions by the Lorentz force. The electromagnetic (EM) field signals emitted by these currents have been studied in different contexts, such as mass transport (Sanford 1971; Larsen and Sanford 1985) and heat flux estimations Larsen and Smith (1992) of ocean currents, the identification and analysis of EM signals generated by Eddies Lilley et al. (1993) or

*Correspondence: petereit@gfz-potsdam.de
[2] Institute of Meteorology, Freie Universität Berlin, Berlin, Germany
Full list of author information is available at the end of the article

passing Hurricanes Sanford et al. (2007). Studies in the field induced ocean-dynamo signals of the general ocean circulation (Vivier et al. 2004; Glazman and Golubev 2005; Manoj et al. 2006; Irrgang et al. 2016b, a), Tsunamis (Toh et al. 2011; Minami et al. 2021; Schnepf et al. 2016; Minami et al. 2015) and ocean tides (Malin 1970; Tyler et al. 2003; Maus and Kuvshinov 2004; Petereit et al. 2018). A comprehensive overview of the recent research in this field was given by Minami (2017).

Ocean-dynamo signals induced through ocean tides are the only ocean-dynamo signals that have been observed from space. The first successful magnetic signal extraction of the diurnal principal lunar tide (M2) from CHAMP data was achieved by Tyler et al. (2003). Since then, additional partial tides (N2, O1) have been extracted successfully (Sabaka et al. 2016; Grayver and Olsen 2019).

Three factors determine the signal strength of tidal ocean-dynamo signals (TODS): the electrical seawater conductivity σ, the tidal current velocities v, and the Earth's magnetic field strength B_{Earth} (mainly the radial component). In the open ocean, changes in the amphidromic system and magnetic field are slow compared to changes in the conductivity distribution which is determined by seawater salinity and temperature. As a result, TODS inferred from satellite data can be used to observe large-scale changes in the oceanic conductivity distribution. These prospects and the fact that state of the art model predictions of M2 TODS Velímský et al. (2018) agree well with satellite observations (Sabaka et al. 2015; Grayver and Olsen 2019), inspired model-based investigations of the effect of conductivity changes on TODS (Saynisch et al. 2017, 2016; Petereit et al. 2018).

Far off the coast Schnepf et al. (2018) and at the ocean bottom Schnepf et al. (2014), M2 TODS identified in magnetometer observations are in good agreement with model predictions. In coastal regions, this is different. Maus and Kuvshinov (2004) and Schnepf et al. (2018) have extracted TODS from coastal island magnetometer data and found an unexplained offset between modeled and observed signal amplitudes. Ocean tides are well observed and hence well understood and predictable. TODS, in contrast, are not. In contrast to sea level data, where the signal of the ocean tide as the dominating signal is easily observed and extracted, the tidal ocean dynamo signal is not easily observed. With a magnitude of at most 10 nT (Nanotesla), TODS are only one of many contributions. In addition, TODS are several orders of magnitude smaller than other magnetic field contributions such as the core magnetic field of the order of 10^4nT and occur at the same frequency range as ionospheric signals. Presently, the shape and time course of TODS are only known to a limited extent.

The reason for the uncertainty is fact that the variability in the conductance, i.e., the depth-integrated conductivity, is more significant in shallow shelf regions than in the open ocean Petereit et al. (2019). Consequently, coastal TODS amplitudes vary significantly on seasonal to decadal time scales. Mainly two effects cause this. On the one hand, seasonal thermocline depth variations Petereit et al. (2019) cause conductance deviations of $\approx$ 10% from the annual mean. On the other hand, thermosteric variations lead to tidal velocity amplitude changes in the order of 10% Müller et al. (2014). In theory, both effects accumulate and cause even larger seasonal TODS variations. Furthermore, in coastal regions, nonlinear effects such as wave interactions with the bathymetry, friction, and wave surges are known to alter the sinusoidal shape of shallow tidal waves. The impact on coastal TODS is currently unknown.

The high variability of coastal TODS on seasonal time scales is momentarily not observable with spaceborne techniques. Until now, M2 TODS amplitudes were only successfully extracted from more than a year of Swarm satellite observations. However, more importantly, small-scale features of TODS are not captured at satellite altitude. The EM signal decay with distance is proportional to $1/r^{(\ell+2)}$. The spherical harmonic degree ℓ is inversely proportional to the length-scale of the signal which implies that large-scale features dominate at satellite altitude Grayver et al. (2016). Consequently, ground-based observations have to be analyzed to learn more about the actual temporal behavior of TODS. We build on the work of Maus and Kuvshinov (2004) and Schnepf et al. (2018) and attempt an evidence-based characterization of temporal TODS variations to contribute to a better understanding of TODS.

For that reason, in this study, we analyze time-series data of 10 years length from three island magnetometer observatories, namely, Ascension Island (ASC), the Crozet Archipelago (CZT) and San Juan on Puerto Rico (SJG). This paper is divided into four parts. The first part presents the data selection criteria and processing methods to filter low-frequency signals of electromagnetic phenomena in the data ("Data selection & processing" section). In the second part, we conduct a spectral analysis on the unevenly sampled residual data to validate our data processing method's advantages compared to existing processing methods ("Spectral analysis" section). In addition, we attempt to identify seasonal M2 TODS variations in the detailed structure of the obtained spectra. In the third part, we apply three existing approaches used to identify M2 TODS in magnetometer observatory data. The results are subsequently compared to assess the robustness of our results and estimate uncertainties ("Trends in M2 tidal signals" section). In the final part

of the presented study, we put our findings into the context of other studies and discuss opportunities for future studies ("Conclusions" section).

Data selection and processing

Data selection and filtering

For this study, we analyzed magnetic field observations from island coastal magnetometer stations found in the INTERMAGNET catalog Love and Chulliat (2013). The chosen time series cover the 10 years 2005– 2015 and are sampled with one averaged observation per minute. The particular stations are situated on Ascension Island (ASC, latitude: −7.95°, longitude: 345.62°), the Crozet Archipelago (CZT, latitude: −46.43°, longitude: 51.87°) and San Juan on Puerto Rico (SJG, latitude: 18.11°, longitude: 293.85°). They were selected through the following criteria. First, the islands lie in ocean regions with high M2 TODS amplitudes Kuvshinov (2008). Second, the coastal proximity of the stations assures a beneficial signal-to-noise ratio which is a precondition for reliable signal extraction. It also increases the chance of detecting seasonal TODS variations anticipated by Petereit et al. (2018). Third, the stations deliver the magnetic field component pointing vertically down (Z, in local Cartesian or cylindrical frames). Ocean tide-induced magnetic fields can be decomposed in their poloidal and toroidal parts. Those two fields differ significantly. Toroidal field components are confined within the ocean and only the poloidal part is measurable outside the ocean in the vertical magnetic field Dostal et al. (2012). Due to the computational costs of the conducted analysis, we limited our choice to three stations.

Separating TODS from magnetic field observations is challenging. Magnetic field measurements integrate signals of various magnetic field sources, such as Earth's lithosphere and core, or currents in the ocean, ionosphere and magnetosphere. The signal strength of all of these signals ranges over several orders of magnitudes and occurs on shared frequency ranges. The strength and variability of the coupled magnetosphere–ionosphere current systems are relatively small during so-called quiet conditions, i.e., the absence of geomagnetic (sub-)storm activity. Much work has been invested into the development of geomagnetic activity indices based on which global/local quiet conditions may be identified (Kp, Dst or Rc index) Kauristie et al. (2017). We follow the lead of Grayver and Olsen (2019) and Schnepf et al. (2018) and identify these quiet conditions with the criteria that Kp$<$ 2 and $\|dDst/dt\| < 2nT/h$ (Matzka et al. 2021; Nose et al. 2015).

The remaining ionospheric signals such as the solar quiet (Sq) current system or ionospheric tides are the largest on Earth's dayside. During the night, the conductivity of the ionosphere plummets to $\approx 1/30$th of its dayside value Malin (1970). We consequently limit our work to the analysis of night-side data. Following the approach of Maus and Kuvshinov (2004), we identify night-side data by identifying time windows in which the average magnetic signal strength is lowest (ASC (6-h window): 9 pm–3 am; CZT (7-h window): 5 pm–0 am; SJG (6-h window) 0 am–6 am (in universal time UTC)). There is also the possibility to identify night-side data as observations when the solar elevation angle Woolf (1968) is several degrees (usually 10) below the horizon Grayver and Olsen (2019). We applied both approaches and found that the first simplified the removal of signals of ionospheric activity in equatorial proximity shortly before sunrise.

Removal of low-frequency variations

After the data processing, the most significant contributor to the remaining signal is the slowly varying core magnetic field. Removing this signal is necessary to isolate the high-frequency TODS and leverage the advantage of their periodicity to the full extend in the subsequent analysis. Identifying and separating periodic signals with high accuracy in long-time series is only possible when low-frequency variations are absent. However, the reliability of the separation depends on the number of cycles included in the time series. Since we are looking for temporal variations of amplitudes and phases in time, we have to ensure that amplitudes and phases are extracted with the highest possible accuracy. This way, we assure that the obtained temporal variations cannot be attributed to other sources.

The influence of low-frequency variations in the observed magnetic field has been dealt with in different ways. For short time series, i.e., in the range of months, it has been assumed that these influences are negligible and have, therefore, been approximated as constant in time Schnepf et al. (2018). For time series in the range of a few years, slow variations have been accounted for by including low frequencies in the harmonic analysis Schnepf et al. (2014). This, however, does not account for non-periodic slow variations such as the secular variation and is thus not suitable for the case at hand.

In the following, we will apply three different approaches to the data obtained from the first processing step: (1) Magnetic field model subtraction, (2) First order differencing and (3) Subtraction of smoothing splines. In the following, we are going to describe all three approaches. The results obtained with these approaches are presented, compared and evaluated in

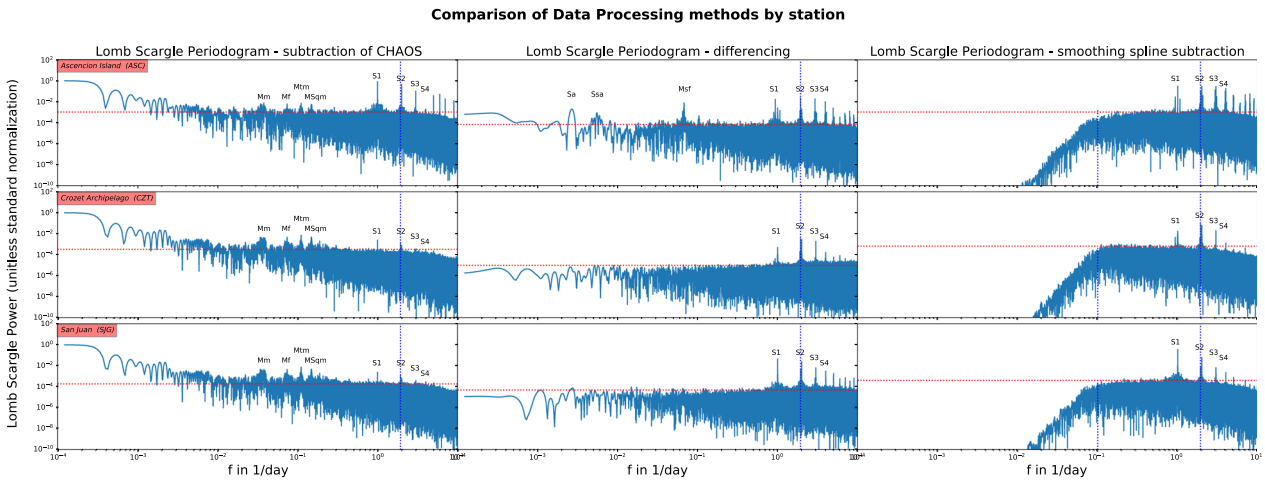

Fig. 1 Lomb–Scargle Periodograms of the residual time series data at all three analyzed Intermagnet stations ASC (top row), CZT (middle row) and SJG (bottom row)). In each column a different removal technique was applied: the subtraction of the model prediction of the CHAOS model (left), differencing of subsequent data points (middle) and the substraction of a smoothing spline (right). Dotted red lines indicate an estimation of the noise level. The dotted blue lines visualize the frequency of the prinicipal lunare tide M2. Other prominent frequency peaks or well-known tidal frequencies are marked with their tidal code, e.g., Sa, Ssa or Mf. The halved dotted blue lines in the right column indicate the targeted cutoff frequency for the smoothing spline ($10^{-1}\mathrm{d}^{-1}$). The amplitudes, noise level and distribution of significant peaks vary as expected with the location due to differing coastal, oceanic and geographical conditions. However, the distribution of detected periodic signals and their signal strength varies with the chosen processing method. Histograms of the residual data obtained from the presented data processing after subtracting smoothing splines are included in the Additional file 1: Figures S1-S3.

"Comparison of data processing procedures" section. and Fig. 1.

Magnetic field model subtraction

The removal of Earth's core can be achieved with the subtraction of model predictions. Examples for available magnetic field models are CHAOS (Finlay et al. 2016, 2020), GRIMM (Lesur et al. 2008, 2010) and the Kalmag model Baerenzung et al. (2020) but also the International Geomagnetic Reference Field (IGRF) (Thébault et al. 2015; Alken et al. 2021), a composite of such individually developed models. Please note, some of these models include the time constant contribution of the Earth's lithosphere, while others do not, e.g., the IGRF. Consequently, eliminating the magnetic field contribution has to be handled differently depending on the chosen model. In our case, we subtracted the CHAOS model predictions (Version 7.6) from the filtered data, such as Grayver and Olsen (2019). Other models deliver comparable results for local magnetic field observation time series as those obtained from the chosen island observatories.

Subtracting a geomagnetic field model is reliable for global magnetometer observations obtained from satellite missions, such as Swarm or CHAMP. At satellite altitude, a lot of the TODS complexity has been reduced due to the stronger decay of small-scale signals with distance.

First-order differencing

A second approach to the problem is using time series analysis (TSA) methods. Typically, TSA methods analyze the statistical properties of stationary time series, i.e., time series with time-constant statistical properties, such as the average or variance. One method to transform non-stationary time series, such as the time series at hand, into a stationary time series is called differencing (Blackman and Tukey 1958a, b; Thomson and Emery 2014).

By subtracting successive magnetic field observations $y(t_i)$:

$$\Delta y(t_i) = y(t_{i+1}) - y(t_i),$$

we obtain a time series of differences $\Delta y(t_i)$ that is "prewhitened," i.e., the power was shifted from lower to higher frequencies and the trend thus removed. We thus computed the minute differences between neighboring data points. If the time passed between two successive observations exceeded 1 min, which occurs between the data gaps created with the above-mentioned data selection procedure, the difference was omitted. In addition to removing the slow variations, the approach also amplifies the TODS, the focus of our study.

In general, first-order differencing can only remove linear trends. Depending on the characteristics of the

trend, differences of higher orders need to be applied. A non-linear trend in the time course of the geomagnetic field, the main contribution to the pre-selected data, is to be expected. However, if variations are slow in time, the remaining trends in the residual data are often masked by the increased noise level. This is also the reason why the same technique was applied by Love and Rigler (2014) who analyzed 97 years of hourly mean magnetic field observation data characterized the *magnetic tides* of Honolulu. Differencing can also be applied to remove seasonality, i.e., periodic signals, in time series data. However, in our case, the seasonality was preserved to analyze the periodic TODS.

Smoothing spline subtraction

A third option for removing slow variations in time series is filtering the data with smoothing splines Craven and Wahba (1978). Splines, especially cubic splines, are rigid, smooth and easy to compute. In addition, they are uniquely identified by the number and position of their knots. It is easy to identify two extreme cases for splines fitted to data. The first is the interpolation spline which passes through every given data point and is, therefore, overfitting the data. The other extreme is the linear spline which is, in essence, a linear regression curve and, therefore, only suitable to remove linear trends. Linear trends, however, do not account for the complex temporal development of the secular variation. It is possible to balance between both extremes and identify a cubic spline function with an equidistant knot distribution that fits well to the data but is, due to the rigid characteristics of the splines, not overfitting the data. In our case, we used cubic splines with equidistantly spaced knots. For each time series, the number of knots was determined so that the following smoothing condition was met:

$$\sum_i \left(y(t_i) - spl(t_i)\right)^2 \leq s \cdot N. \tag{1}$$

Here, $y(t_i)$ is the magnetic field observation and $spl(t_i)$ the value of the smoothing spline at a given time t_i and N the total number of observations and s the smoothing parameter.

The smoothing parameter s depends on residual signals' noise level and signal strength in a given time series. Consequently, identifying a suitable s to filter time series with differing noise levels to a chosen cutoff frequency is not automated easily. It has to be calibrated for each time series individually. To filter signals with period lengths exceeding 10 days in the 10-year time series, we used the following values for s for the chosen station data: ASC: s = 2.3, CZT: s = 16.5 and SJG: s = 45.5.

Spectral analysis

A standard method to assess the periodic variation of time series is to interpret the power spectrum or periodogram. A power spectrum can be computed with the efficient Fast Fourier Transformation (FFT) in an evenly spaced time series. The applied data processing (cf. "Trends in M2 tidal signals" section) removes the disturbing signals but leaves an unevenly spaced time series. Analyzing such time series is common practice in astrophysics, where observations depend on external factors, such as cloud coverage. A standard method to compute a periodogram was developed by Lomb (1976) and later refined by Scargle (1982), the Lomb–Scargle Periodogram (Press et al. 2007; VanderPlas 2018). The Lomb–Scargle method is more demanding on computational resources and time than the FFT method, but the efficiency of the available implementation has dramatically improved, since the algorithm was first developed (Virtanen et al. 2020; Harris et al. 2020).

The Lomb–Scargle Periodogram helps to estimate the spectral power of a harmonic signal of a given frequency. For the data processing, it was used to identify suitable values for the smoothing parameter s by visualizing its impact on the periodogram (cf. Fig. 1). However, it relies essentially on a least-squares algorithm. In addition, the obtained values in the periodogram do not represent the power but a unitless standard normalization P. P is normalized with the variance of the input data. Even though P is closely related to the signal power and signal-to-noise ratio, it is not possible to translate the obtained values directly into physically meaningful ones. However, periodograms are valuable tools for identifying periodic signals (peaks) and their temporal variation (peak shapes and sidebands).

Comparison of data processing procedures

The spectral analysis allows to compare the periodograms of the residual data after applying the three detrending methods (cf. Fig. 1). Judging from the the fact that all images exhibit prominent signal peaks at periods of an integer fraction of a solar day (marked with S_n), the dominating signal found in the residual data is the daily variation. The sum of the individual S_n signals signify the daily variation which can be attributed to mainly solar causes.

There are two kind of tides: gravitational and radiatonal or thermal tides. For gravitational tides, the largest signal is usually the diurnal principal lunar tide M2. This is because the gravitational pull of the moon makes up, depending on the relative position of the sun and the moon on their individual orbits, 2/3 to 3/4 of the total tidal force. Thermal tides originate from the differential

heating of the sun during night and day. Peaks labeled with S_n are most likely of the latter type (see Fig. 1). Because of the dissimilar distribution of solar radiation during night and day, the daily variation is usually non-sinusoidal. It can, however, be deconstructed into a Fourier series with peaks at higher orders, i.e., multiple frequencies of S_1, such as these found in our residual data. That these signal peaks are found in the nightside data provokes different theories about their origin. One explanation could be electric currents in Earth's crust and mantle which are induced by the daily ionospheric variation. These signals lag the inducing source and are, therefore, present during night times. However, the lag should be only measurable shortly after dusk due to the fact that the external-to-internal induction transfer under the given conditions has a phase smaller than 10 degrees. The persistent nature of the residual signals in all analysed time series indicates that the taken measures are insufficient for a clean separation of the desired signal from other magnetic field variations. A finding that needs to be taken into account when interpreting preceding studies.

Comparing the spectra by trend removal method applied, i.e., comparison by column in Fig. 1, we can assess the suitability of the chosen detrending method. We find that subtracting the geomagnetic field model reduced the slow variations but failed to remove them completely. Residual low-frequency signals in the same order of magnitude as the tidal signal peaks remain. While the approach has been proven to be successful for the extraction of TODS from satellite data, it appears to be unsuitable for regional applications. Comparing the spectra at each station after subtracting CHAOS, we find large S_n signal peaks only in ASC. For the other two stations, S_n signals are much smaller. A possible reason are remaining ionospheric signals in the ASC time series.

For the first order differencing, we can clearly observe the successful removal of slow variations in at least two of the three stations (CZT and SJG). We can also confirm the pre-whitening effect as the signal power in higher frequencies has increased in comparison to the previous method. In the data from Ascencion Island, however, we find signs of an annual (Sa), semi-annual (Ssa) and a monthly synodic fortnightly (MSf) variation as well as a residual low frequency variation. These peaks substantiate the suspicion that residual ionospheric signals cannot be removed entirely with the chosen data processing method. The ionospheric daily variation is known to be sensitive to seasonal variations, Earth's orbit around the sun Canton (1759), the sun magnetic activity cycle Sabine (1857) and the lunar cycle (Kreil 1852; Broun 1874). They are the most likely candidates for the found annual, semi-annual and fortnightly signal peaks. An additional argument for the presence of residual ionospheric signals in the data is the found MSf signal. It typically corresponds to the spring-neap-tide frequency and is usually quite small in comparison to other gravitational tidal constituents Cartwright and Tayler (1971). On shallow coastal regions, nonlinear tidal effects can cause the MSf tide to form into a prominent tidal constituent Pugh (1987). However, the absence of prominent signal peaks for the MSm and Mf tide, at least relative to the signal strength of the MSf tide, indicates that it is unlikely that the MSf signals are induced by oceanic processes. Ionospheric processes are the most likely candidate, especially since Love and Rigler (2014) have found comparable signals in their analysis of the daily geomagnetic variation which included day and night side data.

The third detrending method, the subtraction of a smoothing spline has successfully removed low frequencies while leaving high frequencies practically uninfluenced (cf. Fig. 1). The proposed data processing reliably removed periods below the threshold of $f = 0.1\,\mathrm{d}^{-1}$. This allows the separation of all periodic signals in the subsequent signal extraction (c.f. "Trends in M2 Tidal signals" section) in a time series of the given length.

In addition, we want to emphasize the dependence of the detected signal peaks in the frequency range above 1 d^{-1} on the detrending method. This becomes particularly clear when comparing the sidebands of the signal peaks of the solar tides, or the peaks of higher orders. When substracting CHAOS, the peak distribution exhibits a significantly different characteristic than found in the spectra obtained with the other two detrending methods. Since the foundation of the Lomb–Scargle method is the least squares fitting of sinusoidal functions of different frequencies to a given time series VanderPlas (2018), we conclude that the chosen data processing also has an impact on the basic detectability of periodic signals. By removing virtually all slow variations, we can detect the periodic signal peaks and characterize the individual distribution of each island magnetometer observation easier. In consequence, the attained data quality of the residual time series data fulfills the necessary precondition for the subsequent analysis of signal extraction methods.

The magnitude of oceanic and ionospheric tidal signals depends on the geographic location. This is why, we find that noise levels and spectral peak distribution are unique for every observatory when comparing the spectra by station, i.e., comparison by row in Fig. 1.

Indications for periodic M2 signal modulation

The previous section showed that non-oceanic sources could not be excluded for the found signal peaks, especially for solar tides. Consequently, it is doubtful that the fine structure of the signals can be related to the fine

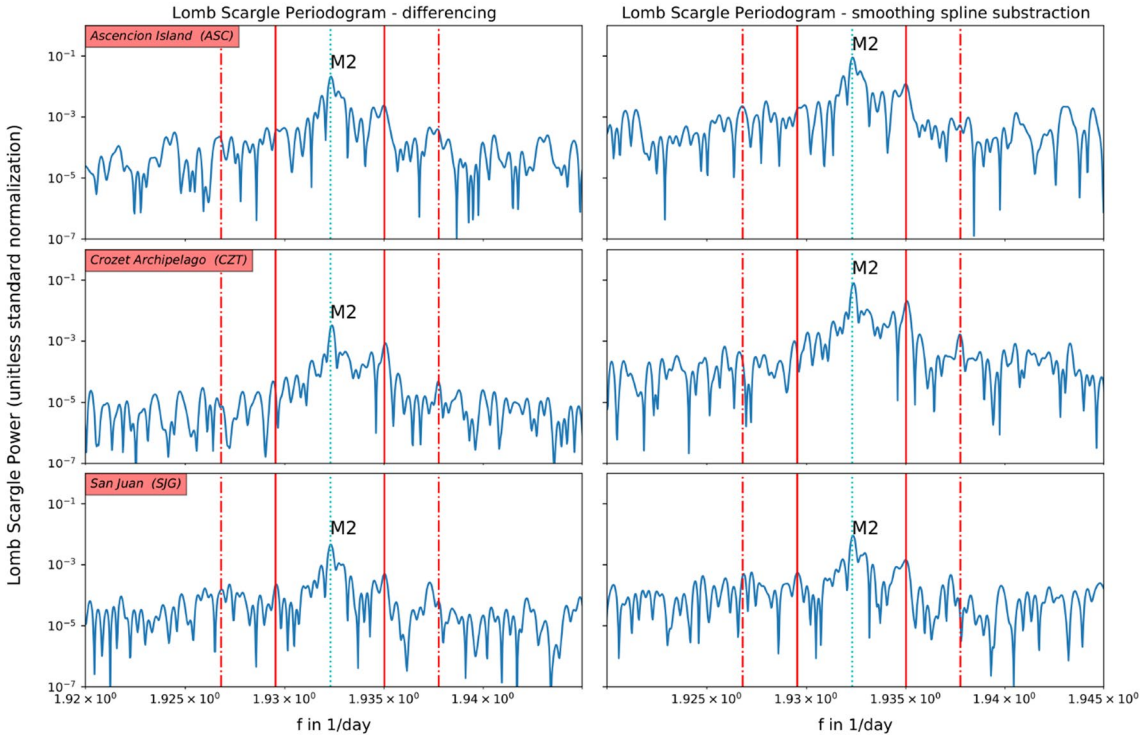

Fig. 2 Comparison of highly resolved periodograms of the M2 TODS peaks at all three analyzed Intermagnet stations ASC (top row), CZT (middle row) and SJG (bottom row). While the left column shows the spectra obtained after first order differencing, the right column shows the results after smoothing spline subtraction. The dotted blue lines mark the frequency of the diurnal principal lunar tide M2. Solid red lines mark side band frequencies associated with an annual variation (Sa) and red dot–dash lines mark side band frequencies associated with a semiannual variation (Ssa). When comparing the left and the right column, we find the hpyerfine structure around the M2 TODS peaks to be independent of the method used for trend removal

structure of ocean tides. However, the semidiurnal principal lunar tide M2 as the most significant tidal component is also larger than the ionospheric counterpart. Therefore, we analyze the detailed structure around the signal peak of tide M2 to identify signs for its seasonal amplitude variation (c.f. Fig. 2). To increase the weight of our findings, we analyze the two residual spectra produced by first-order differencing and smoothing spline subtraction, respectively. Unlike the subtraction of CHAOS, both methods successfully removed slow variations.

From the fields of signal processing and spectral analysis, the impact of amplitude and phase variations on a periodic signal is well-known (Blackman and Tukey 1958a, b). A prominent example is the analysis of sea-level changes that can be obtained from tide gauge data. Here the tide-induced sea-level changes are decomposed into various tidal species. Oceanic tides are mainly gravitational tides that are caused by the interaction of the Earth with the Moon and the Sun. Various components are caused by the periodic variations in the interacting forces due to elliptical and mutually tilted orbits and rotational axis of the celestial bodies (Doodson 1928; Hendershott and Munk 1970). Additional examples are phenomena called beat interference and amplitude modulation. Beat interference is created by two signals with a frequency difference much smaller than the average frequency of both. The frequency of the enveloping signal is similar to the frequency difference of the original signals. The simplest form of amplitude modulation is described as the periodic modulation of a periodic carrier signal which creates symmetric side peaks left and right to the carrier peak frequency, a well-known phenomenon which led to the development of AM (amplitude modulation) radios.

In addition to amplitude and phase variations, the analyzed spectra are affected by additional effects, such as the sampling rate or the time series length. Especially the achievable frequency resolution depends on the sampling. However, while spectra obtained from evenly

sampled data can only resolve frequencies down to the Nyquist limit, this limitation does not directly apply for unevenly sampled data as the conditions from which the Nyquist limit is derived are not met. It is possible to probe frequencies far larger than the Nyquist limit with unevenly sampled data. A demonstration of this as well as a brief overview on attempts to propose Nyquist-like limits for irregular sampling can be found in VanderPlas (2018). Despite that, we find signal peaks with high widths at frequencies corresponding to the M2 tide (f_{M2}) and the side peaks associated with its annual variations, i.e., at the $f_{M2} \pm f_{Sa}$. These broad peaks indicate high variability in the corresponding signals and additional peaks. However, the amount of available data does not suffice to separate these signal peaks. It is reasonable to assume that the global interannual weather variability is also reflected in TODS. It consequently remains to be determined whether these indications for additional variability are artifacts or actual signals originating from periodic variation, trends, or statistical variability.

When comparing the spectra, both detrending methods used provide comparable results (cf. Fig. 2) . The detection probability level of the peaks is higher for the smoothing spline subtraction method. The distribution and proportion of signal peaks are highly similar. In all spectra, we find an asymmetric side peak distribution around the frequencies corresponding to an annual variation ($f = f_{M2} \pm f_{Sa}$), indicating a modulation of both amplitude and phase. There are weak signs for side peaks corresponding to a semiannual modulation ($f = f_{M2} \pm f_{Ssa}$). Since f_{Ssa} is a higher harmonic of f_{Sa}, this is a possible sign for an asymmetric annual modulation. However, the signal strengths of the possible Ssa signal side peaks are more than one order of magnitude smaller than the M2-signal peak. It is, therefore, unlikely that there is a noticeable semi-annual variation in the M2 TODS. On the other hand, the ratio of the M2 signal peak and the side peak found at $f = f_{M2} + f_{Sa}$ are $\approx 3\%$ (ASC), $\approx 25\%$ (CZT) and $\approx 10\%$ (SJG), respectively. The combined signal of the M2 signal peak and the side peaks should add up to a comparable annual variation of the M2 TODS amplitude. Causes for M2 TODS amplitudes variations on annual time scales are variations in ocean tidal velocity amplitudes and the seawater temperature and salinity distribution. For a possible validation of these findings, both effects need to be taken into account.

Trends in M2 tidal signals

In addition to seasonal M2 TODS amplitude variations, we are interested in multi-annual trends, such as the ones investigated by Petereit et al. (2019). The analysis of the spectra alone is insufficient to determine these trends. The achieved level of signal peak separation hinders a definite identification of increasing or decreasing signal amplitudes with time. Especially, since, in addition to a higher resolution, it would also require the analysis of the distributions of real and imaginary components around the M2 TODS peak. Unfortunately, the Lomb–Scargle Periodogram does not provide these data.

To analyze trends in the M2 generated signal amplitudes, we divide the preprocessed 10 year time series into sub-series of increasing lengths and apply three different methods to analyze signal amplitudes. Here we rely on methods that have been used in the past to identify TODS ground-based magnetometer observations (Maus and Kuvshinov 2004; Schnepf et al. 2014, 2018). The chosen approach focuses on insights about the dependence of extracted signal amplitudes on the quantity of available data and, as the temporal behavior of the signal is currently unknown, indications for the temporal variation of M2 TODS. Considering the challenge of separating the M2 TODS with its uncertainties from the residual data, it also allows assessing the dependence of the resulting amplitudes and phases on the chosen extraction method.

For our analysis, it is vital that low-frequency signals were removed from the data. If not, the signals may not be separable from the data. Hence, the detrending methods of subtracting the geomagnetic field model and first-order differencing are unsuitable to meet this precondition, especially for the data obtained at Ascension (ASC) (c.f. Fig. 1). For the following part of the study, we rely thus on the residual data obtained after subtracting smoothing splines.

Phasing and averaging

The first method we applied to identify M2 TODS amplitudes is called phasing and averaging. In this method, each data point is transformed to a new time coordinate related to the phase of the M2 oscillation. The continuous time axis is thereby transformed into a periodic time axis of M2 period length (12h and 25 min). The now overlapping data points are averaged for each minute on the axis. We computed the averages using the arithmetic mean and the median (cf. Fig. 3).

The unique period lengths of the different tidal components create an ever-growing phase shift between the M2 and other tides with each completed oscillation. Assuming that TODS are symmetrical oscillations around the zero value, the signals of tidal constituents other than multiples of the M2 tide are canceled out in the averaging process in long time series. If we further assume that the noise is normally distributed with zero mean, only the mean signal of the M2 tide will remain in the averaging process. We estimate the amplitude from the obtained sinusoidal curve as the halved peak-to-peak difference.

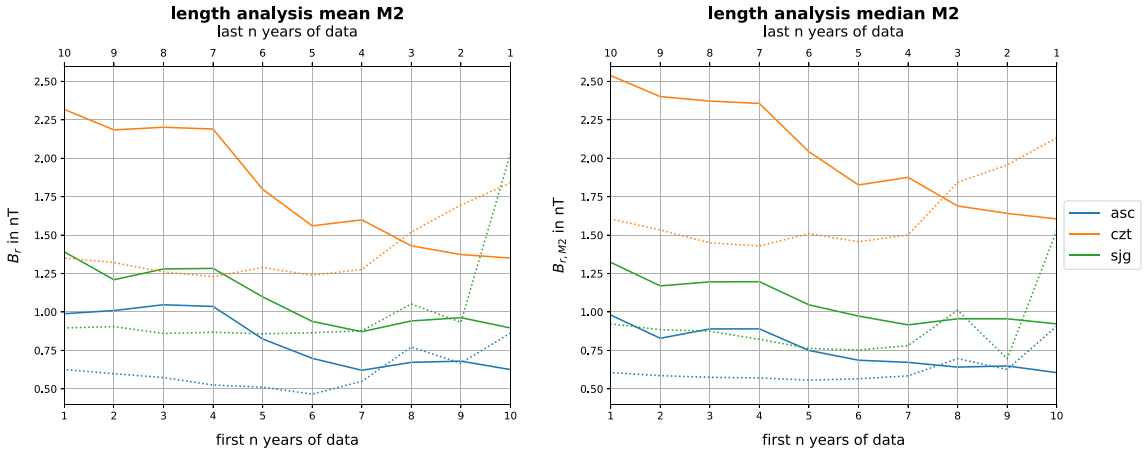

Fig. 3 Oceanic M2 tide induced magnetic field amplitudes in dependence of analyzed time series length at all three analysed coastal magnetometer stations. The amplitudes were obtained after phasing and averaging the data with the mean (left) and the median (right). Solid lines show the results for the analysis conducted on the first *n* years of the 10 year time series (corresponding to lower x-axis), while the dotted lines show the analysis results for the last *n* years of data (corresponding to upper x-axis)

The method is easily implemented and delivers fast results. However, we also want to emphasize the following drawbacks. Due to the made assumptions, it is only applicable if the pre-processing of the observational data can successfully remove all residuals of slowly varying signals. In addition, the smoothness of the obtained sine-shaped average signal depends on the length of the considered time series, the signal-to-noise ratio, and residual signals' presence and strength. Consequently, signal separation becomes more accurate when analyzing long time series and the influence of seasonal and inter-annual variation decreases. The sinus-shaped average signals thus get smoother with time. Furthermore, the method only provides a rough estimate of the average amplitude but does not account for a possible phase shift of the M2 TODS. This means that a phase shift may mask an increase in the amplitude in long time series and vice versa.

For the analysis of the 10 year time series, we started with time series of 1-year length and increased the size incrementally by 1 year. This was done forward in time, starting with the first year, and backward in time, beginning with the last. The results of this analysis are shown in Fig. 3. When comparing the results obtained using the mean and median, we find a consistent amplitude decrease in both methods for all three observatories. However, for the difference in the magnitude of obtained M2 TODS amplitudes, we find a dependency on the selected station. While the difference between mean and median derived amplitudes is consistently large at CZT throughout the entire time series($\approx$ 0.25nT for all time series length), the difference at ASC and SJG decreases with time (from $\approx$ 0.1nT for time series of up to 5 years to almost 0 for more extended time series). When analyzing the time series data (not shown), we find an asymmetric oscillation around the zero-axis in the obtained signal after averaging with the mean, which is not present in the median. Since an offset between median and mean usually indicates a skewed distribution of the given data, we assume that there is either systematic signals in the data which have not been accounted for in the data processing or coastal effects causing distortion or shift of the sinusoidal signal form. One example of such an effect is the presence of ocean currents causing tidal velocities to shift away from the zero baseline, a phenomenon often found in estuaries.

Focusing on the results of the forward analysis, we find that amplitudes decrease with time-series length, which suggests a decrease in all amplitudes over time. This finding is supported by the results obtained from the backward analysis. When comparing the average amplitudes in the first 5-year period (forward analysis) to those of the last one (backward analysis), we find that average amplitudes in the first are indeed larger than those of the last 5-year period. All in all, this validates that there is indeed a perceivable decrease in the amplitudes at the chosen station. However, the large jumps between consecutive years in the first 4 years of the analysis (forward and backward) demonstrate the considerable uncertainty of the method for short time series. Phase shifts, however, have not been analyzed with this method. In principle, this is possible by fitting a sinusoidal model to the obtained averaged sinusoidal curves, but it would add only little value when evaluating the other methods. Then

again, the phase can not be neglected, neither as a possible source for the observed TODS temporal behavior nor as a defining feature of this temporal behavior. Especially, since Saynisch-Wagner et al. (2020) have established the relation between changes in the geomagnetic field and ocean conductivity.

Least squares

The second extraction method is fitting a function $F(t)$ to the residual time series data employing the least-squares method. The fit functions $F(t)$ are model the amplitude of TODS over time. Mathematically they are constructed as sums of harmonic functions related to varying tidal constituents, such as the S1, S2, M2. They have the form:

$$F(t) = \sum_n A_{Tide} \sin(\omega_{Tide} \cdot t) + B_{Tide} \cos(\omega_{Tide} \cdot t). \tag{2}$$

$F(t)$ models the amplitude of ocean tide induced magnetic field signals at a given time t using a sum of harmonic functions with tidal frequencies ω_{Tide}. Equation (2) uses only radial components of the magnetic field, since TODS are only measurable in vertical direction outside of the ocean (cf. sec.). The index *Tide* indicates the tidal constituent, such as S_1, S_2 or M_2. The free parameters A_n and B_n are determined by the least-squares fit. From these coefficients, we compute the TODS amplitude $B_{r,n}$ and also the phase ϕ_n of each tidal mode as

$$B_{r,Tide} = \sqrt{A_{Tide}^2 + B_{Tide}^2} \tag{3}$$

$$\phi_{Tide} = \begin{cases} \arctan\left(\frac{B_n}{A_{Tide}}\right) & \text{if } A_{Tide} > 0, \\ \arctan\left(\frac{B_{Tide}}{A_{Tide}}\right) + \pi & \text{if } A_{Tide} < 0 \text{ and } B_{Tide} > 0, \\ \arctan\left(\frac{B_{Tide}}{A_{Tide}}\right) - \pi & \text{if } A_{Tide} < 0 \text{ and } B_{Tide} < 0, \\ \frac{\pi}{2} & \text{if } A_{Tide} = 0 \text{ and } B_{Tide} > 0, \\ -\frac{\pi}{2} & \text{if } A_{Tide} = 0 \text{ and } B_{Tide} < 0, \\ \text{undefined} & \text{if } A_{Tide} = 0 \text{ and } B_{Tide} = 0, \end{cases} \tag{4}$$

.

We fitted eight different functions $F(t)$, or *models*, to the residual time series. Each fit function differs in the number and choice of tidal constituents used to fit the data. The only constant is the fit of the tidal frequency of the M2, the principal lunar tide. Details about the composition of tidal components in each model and exact values of corresponding tidal frequencies used can be found in the Additional file 1. In general, the fit function can be classified into two groups. The first group focuses on fitting the M2 tide, either alone or together with its variations. There, functions include only frequencies corresponding to the M2 tide, its overtides and cyclical amplitude variations, such as semi-annual variation. The simplest example models signal of the M2 tide using two parameters (A_{M2} and B_{M2}; it is similar to the M2 amplitude determination method for coastal island magnetometer observations of Maus and Kuvshinov (2004). The most complex model in this group, called "M2_overtides_modulation", includes overtides and their seasonal variation using 240 parameters. Cyclical amplitude modulations are modeled by including sidebands of long periodic modulation frequencies f_{mod} corresponding to annual and monthly variations. Mathematically, the sidebands are formulated as

$$f_{M2,mod} = f_{M2} \pm f_{mod}$$

The second group of fitting functions is based on the models used by Schnepf et al. (2014) or by the National Oceanic and Atmospheric Association (NOAA). In addition to the frequencies corresponding to the principal lunar tide M2 and its overtides or modulations, further tidal components such as the O1 or S2 are included. While the "Schnepf_2014" model includes 15 tidal components, the "NOAA" model consists of the 37 constituents which usually have the most significant effect on oceanic tidal sea-level signals (Schureman 1958; Parker 2007). Both of these models naturally include low-frequency tides. In theory, these should not be present after the data processing. Hence, the second group of models additionally compares the influence of excluding low-frequency tides on the amplitude of the M2 tide with models containing the suffix "_short."

The results of the analysis with the simple least-squares method are summarized in Fig. 4. To ease the comparison between the phasing and averaging and the least-squares method, we included the results of phasing and averaging as black lines.

To investigate the robustness of this method, we first focus on the convergence behavior of the presented curves with time-series length. One finding is that the curves of all measured variables, amplitudes and phases alike, converge. Except for the amplitudes identified in the ASC data. The phases are, in general, very robust and all fit functions seem to converge to nearly the same values in few years. For the amplitude curves in CZT and SJG, the fit functions converge after 2 and 4 years, respectively. 4 years also appears to be the time when the difference between the phasing and averaging and the least-squares method becomes negligible. The dependency of shorter time series on the fitting function indicates that signals have not been separated sufficiently.

When focusing on the temporal progression of the curves, we see a change in both amplitudes and phases, a finding that is supported by the comparison of forward and backward analysis (cf. "Phasing and averaging"

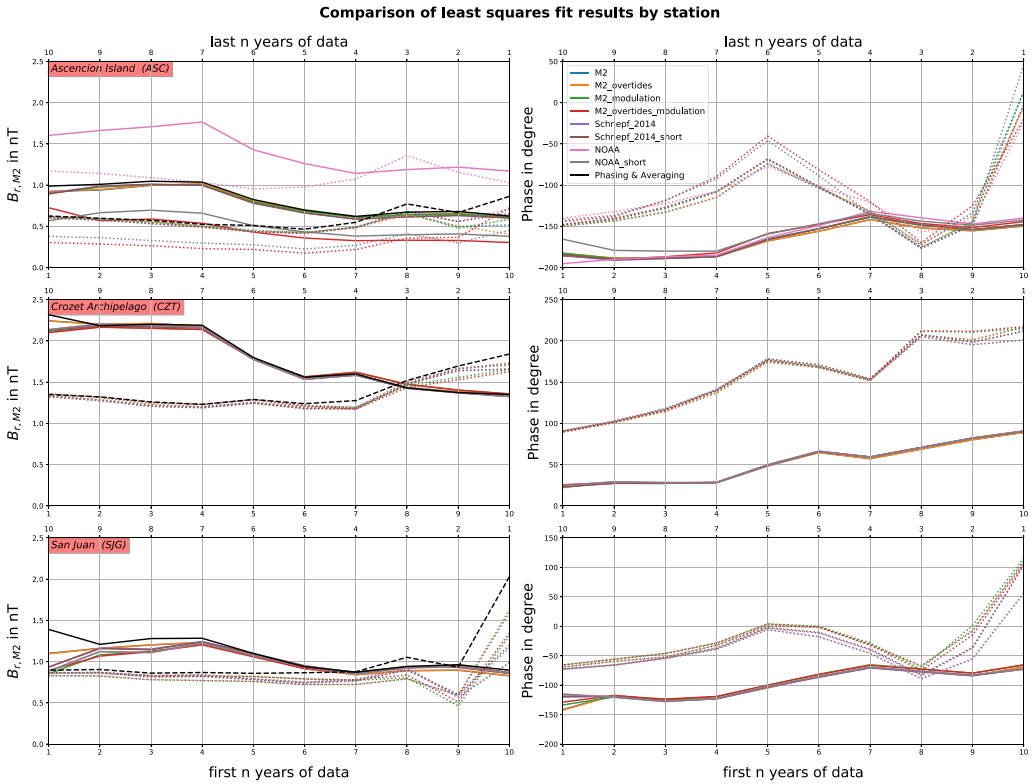

Fig. 4 Comparison of oceanic M2 tide induced magnetic field signal parameters extracted from the residual data with *least squares fitting* of different harmonic sums. The left column shows the extracted amplitudes and the right column the extracted phases in dependence of analysed time series length. While solid lines show the results for the analysis conducted on the first *n* years of the 10 year time series (corresponding to lower x-axis), dotted lines show the analysis results for the last *n* years of data (corresponding to upper x-axis). Black lines in the left column show the results obtained by phasing and averaging the residual data and allows for a comparison of both methods. Please note, on the right-hand column the y-scales vary by row. This choice was made to increase presentability of the obtained results. Root mean square values of the residual data for each data point, i.e., for each the fit made with each fit function to the given time span is summarized in the Additional file 1 under Tables S6–S11

section). While changes of the average amplitudes are in the order of $\mathcal{O}(0.1\text{nT})$, changes of the phase are in the order of $\mathcal{O}(10°)$ and reach values of more than 100° in all three observatory time series for the backward analysis. The temporal variation of the M2 phases is to be expected Saynisch-Wagner et al. (2020). In all time series, the temporal progression of the amplitudes is very similar to the one found with the first method.

Judging from the spectra after the data processing in "Comparison of Data Processing Procedures" section. and the comparison of values obtained after using the mean and the median in "Phasing and Averaging" section , there is no apparent difference in the quality of the three data series. All the more surprising is that the amplitude curves obtained from the ASC data do not converge, especially since the phases do. We find a cluster of curves delivering values similar to method one, but some curves such as the ones corresponding to the label “NOAA” and “M2_overtides _modulation” show a consistently large offset in the forward and the backward analysis. These functions are also quite distinct as the former consists of the sum of the most common partial tides and the latter of a sum of Mx-Tides, i.e., M2 and its overtides, and their temporal variation. In addition, they deliver reliable results for the observations at CZT and SJG. Furthermore, they agree with the general temporal progression of all curves. Therefore, we can only speculate about residual signals in the data interfering with our analysis. A likely origin for these signals is the ionosphere, as we identified signs of ionospheric signals after the detrending methods of first-order differencing and magnetic field model subtraction in ASC (cf. "Comparison of Data Processing Procedures" section).

A major shortcoming of the least-squares method is its sensitivity to the existence of outliers. The implied assumption of the least-squares method is that errors are normally distributed. Thus the likelihood of extreme outliers occurring is very small. The least-squares approach is very efficient in time series with

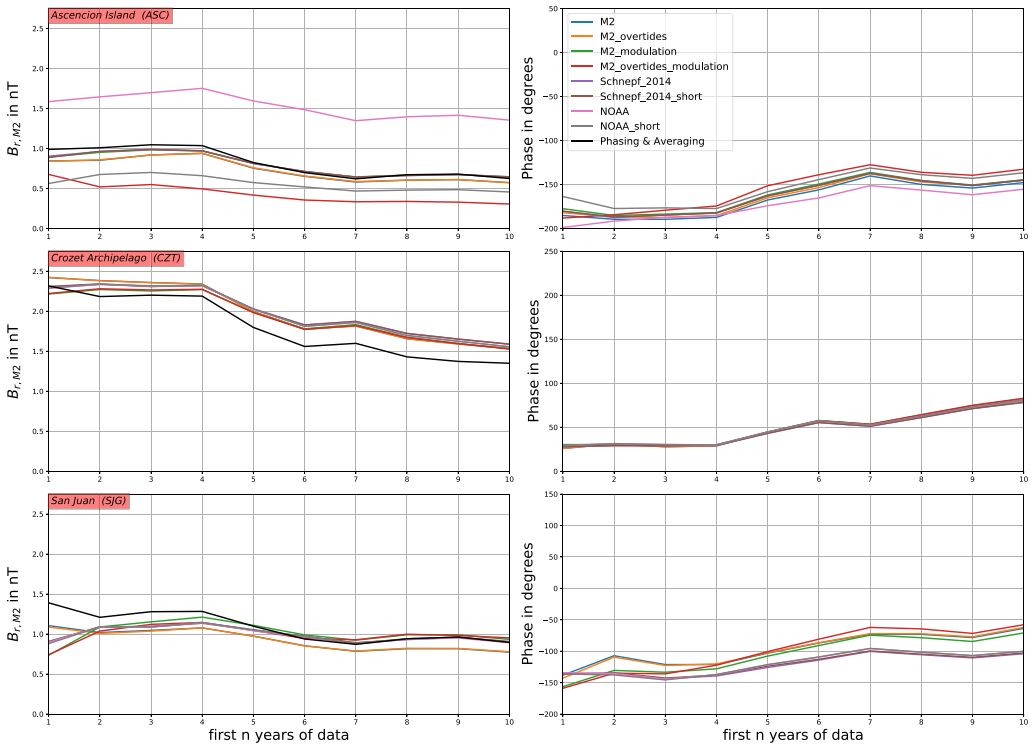

Fig. 5 Comparison of oceanic M2 tide induced magnetic field signal parameters extracted from the residual data by fitting different harmonic sums using an *iterative robust least squares* approach. The left column shows the extracted amplitudes and the right column the extracted phases in dependence of analysed time series length. In contrast to the previous figures, only the analysis of the first *n* years of the 10 year time series are presented because of the computational costs of this analysis and the evident conclusions that can be drawn from these presented results. Black lines in the left column show the results obtained by phasing and averaging the residual data and allows for a comparison of both methods. Please note, on the right-hand column the y-scales vary by row. This choice was made to increase presentability of the obtained results. Root mean square values of the residual data for each data point, i.e., for each the fit made with each fit function to the given time span is summarized in the Additional file 1 under Tables S12–S14

few outliers and fully explained signals. Nevertheless, it is unlikely that a pre-defined fitting function applied to all measuring sites accounts for local differences in TODS, especially when we consider the dissimilarities among the three residual time series, Fig. 1), the challenge of separating signals using short time series and when taking into account that temporal varying amplitudes and nonlinear effects cause further signal peaks.

Robust least squares

On account of the least-squares method being overly affected by outliers, its general concept was advanced into an iteratively reweighted least-squares (IRLS) (Holland and Welsch 1977; Huber 2004). The IRLS is an iterative optimization approach that reduces the impact of outliers on the overall fit. For details on the setup of the algorithm, we refer to Schnepf et al. (2014), Schnepf et al. (2018) as we followed their lead for the implementation of the third extraction method used in this study.

We used the same eight fitting functions as in the previous section. The approach is computationally very expensive, especially when minimizing fit functions with up to 240 parameters with 10 years of average observations for every minute within the time series. The results obtained with the forward analysis are sufficiently conclusive. Since the backward analysis does not provide additional value, we omitted it consequently for this part of the study. The results are summarized in Fig. 5.

Comparing Figs. 5 and 4, we see the same qualitative temporal behaviour of mean amplitudes and phases. We also find that phase values are in general less sensitive to the chosen fitting function which indicates an increased robustness of phase values over amplitude values. However, apart from these similarities, we find a considerable deviation in the convergence behavior of both amplitudes and phases. While differences between phases were in the order of $\mathcal{O}(5°)$ in all stations when analysing time series longer than four years with the ordinary least squares

approach, there is no apparent generalized behaviour when using the IRLS for the analysis. While at CZT the phase values converge almost immediately and deviate by a few degrees, at ASC we have an almost constant spread of $\approx 20°$. At SJG the individual phase curves form a group with a total spread of $\approx 30°$. Also for the amplitudes, we find a larger spread. The spread at ASC stays large with a value of $\approx$ 1nT. The spread at CZT converges after ≈ 4 years to a group of curves with a spread of $\approx$ 0.1nT. For SJG, we find that amplitudes conserve an almost constant spread of $\approx$ 0.2nT. In addition, the curves obtained from the SJG data are seemingly separated into two groups for both, amplitudes and phases. This indicates that the algorithm may not be able to identify a global minimum on a flat curve with several local minima.

All in all, we find it plausible that there seems to be a correlation between amplitude M2 signal strength (largest at CZT) and the observed spread in amplitude and phase. Strong signals are generally easier to identify. The "Phasing and averaging" section already indicated a systematic influence of additional signals on the TODS induced by the M2 tide. In view of these results, we find plausible that the amplitude curves obtained from the CZT data converge to a curve with a substantial offset from the curve obtained by averaging the phased data using the mean.

A possible reason for the noticable divergence of the results obtained from the analysis of the ASC data in comparison to the data of the other observatories is the location. In contrast to CZT and SJG, ASC is located in proximity of the geomagnetic equator. Here, the radial magnetic field is much smaller which leads to the fact TODS amplitudes largely defined by the radial geomagnetic field component are reduced to almost zero. With the decreased amplitude, external influences have a larger relative impact which may increase the challenge of a clean signal separation. Hence, for future attempts to analyse TODS originating from coastal island magnetometer data requires designing suitable fit functions for each observatory individually.

Conclusions

In principle, it is possible to use ocean tide-induced magnetic field signals for ocean observation purposes. The signals contain integrated information about seawater temperature and salinity, tidal transports and the strength of the radial geomagnetic field component. As the ocean is largely under-observed spatially and temporally in all physical relevant quantities, such as temperature and salinity and oceanic transports, the signals are a promising asset in closing the observation gap in the ocean. From model studies (Petereit et al. 2019; Saynisch-Wagner et al. 2020), it is known that in coastal regions oceanic warming and seasonal thermocline displacements cause considerable variations in both tidal ocean dynamo signal (TODS) amplitudes and phases. These observation regions are consequently of particular significance for ocean observation purposes. However, ground-based observations in those regions show a noticeable offset between observed and modeled ocean tide induced magnetic field amplitudes (Maus and Kuvshinov 2004; Schnepf et al. 2018). Out of several explanations, one is the fact that the radial magnetic field in coastal proximity is largely influenced by the surrounding 3-D conductivity structure of the shore (Dostal et al. 2012; Schnepf et al. 2015). The conductivity structure results from the bathymetry, which defines the amount of conductive seawater and mire, which has to be modeled with adequate resolution to account for this effect. The same is true to account for the high spatial variability of ocean currents in shelf regions, as well as the fact that ocean tide-induced magnetic fields measured at one location can be induced at distant ocean regions Young et al. (1920). Another explanation for this mismatch is uncertainties in the signal characterization. The aforementioned increased variability of ocean tide-induced magnetic field amplitudes and phases in coastal regions and their sensitivity towards changes in the geomagnetic field create, as temporal TODS variations have not been investigated to this date, an additional uncertainty (Additional file 1).

In this study, we add to the characterization of TODS by identifying indications for temporal TODS variations in 10 years of minute magnetometer data. In particular, the data of three island magnetometer observatories was investigated. We first evaluated the quality of different data processing approaches with a spectral method capable of analyzing the unevenly sampled data obtained after the processing. We find that existing approaches, namely, subtracting geomagnetic core field models, such as, in our case, CHAOS or applying first-order differencing, show deficiencies. After presenting and evaluating a suitable data processing technique, we used the data to assess seasonal variations and long-term trends. For the seasonal variations, we assessed the signal strength of M2 signal peak sidebands in the spectral data. We find indications for seasonal variations from the mean annual mean amplitude of, depending on the measuring site, from $\approx$ 3% to $\approx$ 25% of the M2 signal strength.

For the long-term amplitude and phase trends, we used three approaches to identify mean amplitudes and phases in the time series data. The approaches were applied to time series of incrementally increasing lengths (increment = one year), starting with a time series length of one year. We find that with increasing lengths, mean amplitudes change by up to $\approx$ 1nT. Average amplitudes

and phases obtained by the used methods differ substantially from actual M_2 TODS amplitudes for the following reasons. Variations and trends in the actual amplitudes are averaged in the extraction methods over the respective time span. It is unknown whether these averaged amplitudes change because of trends, phase changes, interannual variation in the seasonal variability, measurement uncertainties, or a combination of each. The extracted amplitudes are, therefore, an approximation to the actual amplitude. Furthermore, none of the presented extraction methods includes temporal trends in phases or amplitudes a priori. However, based on the findings of this study, it will be necessary to include them in future studies when attempting to model functions that aim at explaining or extracting the contribution of TODS to magnetic field observations. An additional effect that needs to be considered is that, over 10-year time periods, changes in amplitudes and phases of tidal transports vary naturally and reach values of several percent and degrees. These long-term variations in tidal transports can be directly inferred from the ephemerides using existing algorithms. Consequently, the impact of the secular variation of the geomagnetic field, changes in tidal transports, and seawater conductivity variations on seasonal to decadal time scales needs to be considered or even separated in the future (Additional file 1).

Based on our results, we find that when applying the presented methods, more than 4 years of observations are necessary to obtain reliable results. Using these methods, identification of seasonal variations can hence not be achieved. In addition, we find that signal phases do not only show temporal variations in the order of $\mathcal{O}(10°)$ but also appear to be more robust with regards to the chosen fit function than signal amplitudes. However, on account of the need for sub-annual resolution of the temporal variability of the signal, better-adapted methods need to be applied to extract the minute signals from magnetic field observations. A possible start would be the implementation of a more sophisticated fit function Guzavina et al. (2018). However, more promising results are to be expected from the application of other spectral estimation methods, such as Singular Spectrum Analysis (SSA). The spectrum of TODS deviates largely from the spectrum of tidal transports, the source of TODS. An estimation of the complete TODS spectrum and a demonstration of separation of ionospheric signals would make way to an unprecedented level of understanding as the relation between cause and effect can be analyzed reliably in all tidal components.

Advances in this field are relevant for ocean observations and have applications in magnetotelluric studies as they can be used for sounding the conductivity distribution of the mantle. Ocean tide-induced magnetic field signals are sensitive to the conductivity distribution of subsurface layers (Chave 1983; Dostal et al. 2012; Schnepf et al. 2015). This allowed for a successful global inversion to obtain an improved 1-D mantle conductivity distribution Grayver et al. (2016). More important is to realize a comprehensive understanding of the temporal development of ocean tide-induced magnetic field signals in coastal proximity.

One future measure is to advance the modeling capacities to small-scale processes on the coastal shelves. When combining advancements in electromagnetic field modelling Kruglyakov and Kuvshinov (2020) and ocean modelling Sulzbach et al. (2021), improved results are to be expected. In addition, this would also help shed light on the long-range effect of electromagnetic fields in the observed magnetic field amplitudes. Already in 1920, tidal ocean-dynamo signals were measured that did not match the tidal flow at the measurement site, but with the stronger flow at a distant location generating stronger signals Young et al. (1920). Identifying the exact location of the electric source causing the observed magnetic fields or the composition of sources adding to the signal will help bridge the gap between EM signal observation and ocean observation. This is especially important as the remote sensing advantage achieved through spaceborne TODS observations does not apply to small-scale EM signals. They decay faster than large-scale signals with the distance so that at satellite altitude, only the large-scale pattern of the global tides remains. This is also the reason why Tsunamis are unlikely to be detected at satellite altitude even though their signal strength is comparable with those of ocean tide-induced magnetic field signals at sea level Kuvshinov (2008). The challenge of identifying seasonal M2 signal variations in coastal island magnetometer observations and linking them to their oceanic cause remains (Additional file 1).

Supplementary Information

The online version contains supplementary material available at https://doi.org/10.1186/s40623-022-01610-9.

Additional file 1. Additional file to: On temporal variations of coastal tidal ocean-dynamo signals.

Acknowledgements

The results presented in this paper rely on data collected at magnetic observatories. We thank the national institutes that support them and INTERMAGNET for promoting high standards of magnetic observatory practice (www.intermagnet.org). Primarily, we thank the institutes British Geological Survey, United States Geological Survey and École et Observatoire des Sciences de la Terre, for supporting the operation of the observatories our research is based on. Furthermore, we thank the German Research Foundation for funding this study's research in the priority program 1788 "Dynamic Earth". We thank the geomagnetic observatories (Kakioka [JMA], Honolulu and San Juan [USGS],

Hermanus [RSA], INTERMAGNET, and many others for their cooperation to make the final Dst index available. Finally, we want to express our appreciation for the energy and effort the anonymous reviewers have gone through to improve the initial manuscript to its current form.

Author contributions
Each author has made substantial contributions to this work. All authors read and approved the final manuscript.

Funding
Open Access funding enabled and organized by Projekt DEAL. This work has been funded by the DFG within the priority program 1788 "Dynamic Earth"

Availability of data and materials
All the data are available as part of the INTERMAGNET (definite) catalogue. (www.intermagnet.org).

Declarations

Competing interests
The authors declare that they have no competing interests.

Author details
[1]GFZ German Research Centre for Geosciences, Potsdam, Germany. [2]Institute of Meteorology, Freie Universität Berlin, Berlin, Germany. [3]German Aerospace Center, Institute for Solar-Terrestrial Physics, Neustrelitz, Germany.

Received: 22 September 2021 Accepted: 23 March 2022
Published online: 29 April 2022

References

Alken P, Thébault E, Beggan CD, Amit H, Aubert J, Baerenzung J, Zhou B (2021) International geomagnetic reference field: the thirteenth generation. Earth Planets Space 73(1):1–25. https://doi.org/10.1186/s40623-020-01288-x

Baerenzung J, Holschneider M, Wicht J, Lesur V, Sanchez S (2020) The kalmag model as a candidate for igrf-13. Earth Planets Space 72(1):1–13

Blackman RB, Tukey JW (1958) The measurement of power spectra from the point of view of communications engineering—part I. Bell Syst Tech J 37(1):185–282. https://doi.org/10.1002/j.1538-7305.1958.tb03874.x

Blackman RB, Tukey JW (1958) The measurement of power spectra from the point of view of communications engineering—part II. Bell Syst Tech J 37(2):485–569. https://doi.org/10.1002/j.1538-7305.1958.tb01530.x

Broun JA (1874) Observations of magnetic declination made at trevandrum and agustia malley in the observatories of his highness the maharajah of travancore, gcsi in the years 1852 to 1869: Being trevandrum magnetical observations, vol 1. King & Company, Henry S

Canton J (1759) XXXVIII an attempt to account for the regular diurnal variation of the horizontal magnetic needle and also for its irregular variation at the time of an aurora borealis. Philos Trans R Soc Lond 51: 398–445

Cartwright D, Tayler R (1971) New computations of the tide-generating potential. Geophys J Int 23(1):45–73

Chave AD (1983) On the theory of electromagnetic induction in the earth by ocean currents. J Geophys Res Solid Earth 88(B4):3531–3542. https://doi.org/10.1029/JB088iB04p03531

Craven P, Wahba G (1978) Smoothing noisy data with spline functions. Numerische Mathematik 31(4):377–403. https://doi.org/10.1007/BF01404567

Doodson AT (1928) VI. The analysis of tidal observations. Philos Trans R Soc Lond Ser A Contain Pap Math Phys Character 227(647–658):223–279

Dostal J, Martinec Z, Thomas M (2012) The modelling of the toroidal magnetic field induced by tidal ocean circulation. Geophys J Int 189(2):782–798. https://doi.org/10.1111/j.1365-246X.2012.05407.x

Finlay CC, Kloss C, Olsen N, Hammer MD, Tøffner-Clausen L, Grayver A, Kuvshinov A (2020) The chaos-7 geomagnetic field model and observed changes in the south Atlantic anomaly. Earth Planets Space 72:156. https://doi.org/10.1186/s40623-020-01252-9

Finlay CC, Olsen N, Kotsiaros S, Gillet N, Tøffner-Clausen L (2016) Recent geomagnetic secular variation from swarm and ground observatories as estimated in the chaos-6 geomagnetic field model. Earth Planets Space 68:112. https://doi.org/10.1186/s40623-016-0486-1

Glazman RE, Golubev YN (2005) Variability of the ocean-induced magnetic field predicted at sea surface and at satellite altitudes. J Geophys Res Oceans. https://doi.org/10.1029/2005JC002926

Grayver AV, Olsen N (2019) The magnetic signatures of the m2, n2, and o1 oceanic tides observed in swarm and champ satellite magnetic data. Geophys Res Lett 46(8):4230–4238. https://doi.org/10.1029/2019GL082400

Grayver AV, Schnepf NR, Kuvshinov AV, Sabaka TJ, Manoj C, Olsen N (2016) Satellite tidal magnetic signals constrain oceanic lithosphere-asthenosphere boundary. Sci Adv 2:9. https://doi.org/10.1126/sciadv.1600798

Guzavina M, Grayver A, Kuvshinov A (2018) Do ocean tidal signals influence recovery of solar quiet variations? Earth Planets Space 70(1):1–15

Harris CR, Millman KJ, van der Walt SJ, Gommers R, Virtanen P, Cournapeau D, Oliphant TE (2020) Array programming with NumPy. Nature 585:357–362. https://doi.org/10.1038/s41586-020-2649-2

Hendershott M, Munk W (1970) Tides. Annu Rev Fluid Mech 2(1):205–224

Holland PW, Welsch RE (1977) Robust regression using iteratively reweighted least-squares. Commun Stat Theory Methods 6(9):813–827. https://doi.org/10.1080/03610927708827533

Huber PJ (2004) Robust statistics, vol 523. Wiley

Irrgang C, Saynisch J, Thomas M (2016) Ensemble simulations of the magnetic field induced by global ocean circulation: estimating the uncertainty. J Geophys Res Oceans 121(3):1866–1880

Irrgang C, Saynisch J, Thomas M (2016) Impact of variable seawater conductivity on motional induction simulated with an ocean general circulation model. Ocean Sci 12(1):129–136. https://doi.org/10.5194/os-12-129-2016

Kauristie K, Morschhauser A, Olsen N, Finlay CC, McPherron R, Gjerloev J, Opgenoorth HJ (2017) On the usage of geomagnetic indices for data selection in internal field modelling. Space Sci Rev 206(1–4):61–90. https://doi.org/10.1007/s11214-016-0301-0

Kreil K (1852) Einfluss des mondes auf die magnetische declination, vol 1. Kaiserlich-Königlichen Hof-und Staatsdruckerei

Kruglyakov M, Kuvshinov A (2020) Introducing new global electromagnetic modeling solver

Kuvshinov AV (2008) 3-D global induction in the oceans and solid earth: recent progress in modeling magnetic and electric fields from sources of magnetospheric, ionospheric and oceanic origin. Surv Geophys 29(2):139–186

Larsen JC, Sanford TB (1985) Florida current volume transports from voltage measurements. Science 227(4684):302–304. https://doi.org/10.1126/science.227.4684.302

Larsen JC, Smith FT (1992) Transport and heat flux of the florida current at 27 degrees n derived from cross-stream voltages and profiling data: theory and observations. Philos Trans R Soc A Math Phys Eng Sci 338(1650):169–236. https://doi.org/10.1098/rsta.1992.0007

Lesur V, Wardinski I, Hamoudi M, Rother M (2010) The second generation of the gfz reference internal magnetic model: Grimm-2. Earth Planets Space 62(10):765–773

Lesur V, Wardinski I, Rother M, Mandea M (2008) Grimm: the GFZ reference internal magnetic model based on vector satellite and observatory data. Geophys J Int 173(2):382–394

Lilley F, Filloux J, Mulhearn P, Ferguson I (1993) Magnetic signals from an ocean eddy. J Geomagn Geoelectr 45:403–422. https://doi.org/10.5636/jgg.45.403

Lomb NR (1976) Least-squares frequency analysis of unequally spaced data. Astrophys Space Sci 39(11):447–462. https://doi.org/10.1007/BF00648343

Love JJ, Chulliat A (2013) An international network of magnetic observatories. Eos Trans Am Geophys Union 94(42):373–374. https://doi.org/10.1002/2013EO420001

Love JJ, Rigler EJ (2014) The magnetic tides of Honolulu. Geophysical Journal International 197(3):1335–1353. https://doi.org/10.1093/gji/ggu090

Malin SRC (1970) Separation of Lunar daily geomagnetic variations into parts of ionospheric and oceanic origin. Geophys J Int 21(5):447–455. https://doi.org/10.1111/j.1365-246X.1970.tb01781.x

Manoj C, Kuvshinov A, Maus S, Lühr H (2006) Ocean circulation generated magnetic signals. Earth Planets Space 58(4):429–437. https://doi.org/10.1186/BF03351939

Matzka J, Stolle C, Yamazaki Y, Bronkalla O, Morschhauser A (2021) The geomagnetic KP index and derived indices of geomagnetic activity. Space Weather 19(5): e2020SW002641. https://doi.org/10.1029/2020SW002641

Maus S, Kuvshinov AV (2004) Ocean tidal signals in observatory and satellite magnetic measurements. Geophys Res Lett 31:15. https://doi.org/10.1029/2004GL020090
Minami T (2017) Motional induction by Tsunamis and ocean tides: 10 years of progress. Surv Geophys 38(5):1097–1132
Minami T, Schnepf NR, Toh H (2021) Tsunami-generated magnetic fields have primary and secondary arrivals like seismic waves. Sci Rep 11(1):1–8. https://doi.org/10.1038/s41598-021-81820-5
Minami T, Toh H, Tyler RH (2015) Properties of electromagnetic fields generated by tsunami first arrivals: classification based on the ocean depth. Geophys Res Lett 42(7):2171–2178. https://doi.org/10.1002/2015GL063055
Müller M, Cherniawsky JY, Foreman MGG, von Storch JS (2014) Seasonal variation of the M2 tide. Ocean Dyn 64(2):159–177. https://doi.org/10.1007/s10236-013-0679-0
Nose M, Iyemori T, Sugiura M, Kamei T (2015) Geomagnetic dst index. World Data Center for Geomagnetism, Kyoto 10:14–515. https://doi.org/10.17593/14515-74000
Parker BB (2007) Tidal analysis and prediction. NOAA, NOS Center for Operational Oceanographic Products and Services
Petereit J, Saynisch J, Irrgang C, Weber T, Thomas M (2018) Electromagnetic characteristics of ENSO. Ocean Science 14(3):515–524. https://doi.org/10.5194/os-14-515-2018
Petereit J, Saynisch-Wagner J, Irrgang C, Thomas M (2019) Analysis of ocean tide-induced magnetic fields derived from oceanic in situ observations: climate trends and the remarkable sensitivity of shelf regions. J Geophys Res Oceans 124(11):8257–8270. https://doi.org/10.1029/2018JC014768
Press WH, William H, Teukolsky SA, Vetterling WT, Saul A, Flannery BP (2007) Numerical recipes. The art of scientific computing, 3rd edn. Cambridge University Press
Pugh DT (1987) Tides, surges and mean sea level. Wiley, New York
Sabaka TJ, Tyler RH, Olsen N (2016) Extracting ocean-generated tidal magnetic signals from Swarm data through satellite gradiometry. Geophys Res Lett 43(7):3237–3245
Sabaka TJ, Tyler RH, Olsen N, Kuvshinov AV (2015) CM5, a pre-Swarm comprehensive geomagnetic field model derived from over 12 yr of CHAMP, Ørsted, SAC-C and observatory data. Geophys J Int 200(3):1596–1626. https://doi.org/10.1093/gji/ggu493
Sabine E (1857) I. On the evidence of the existence of the decennial inequality in the solar-diurnal magnetic variations, and its non-existence in the lunar-diurnal variation, of the declination at hobarton. Philos Trans R Soc Lond 147:1–8
Sanford TB (1971) Motionally induced electric and magnetic fields in the sea. J Geophys Res 76(15):3476–3492. https://doi.org/10.1029/JC076i015p03476
Sanford TB, Price JF, Girton JB, Webb DC (2007) Highly resolved observations and simulations of the ocean response to a hurricane. Geophys Res Lett 34:13. https://doi.org/10.1029/2007GL029679
Saynisch J, Petereit J, Irrgang C, Kuvshinov A, Thomas M (2016) Impact of climate variability on the tidal oceanic magnetic signal—a model-based sensitivity study. J Geophys Res Oceans 121(8):5931–5941
Saynisch J, Petereit J, Irrgang C, Thomas M (2017) Impact of oceanic warming on electromagnetic oceanic tidal signals: a CMIP5 climate model-based sensitivity study. Geophys Res Lett 44(10):4994–5000
Saynisch-Wagner J, Petereit J, Irrgang C, Thomas M (2020) Phase changes of electromagnetic oceanic tidal signals. J Geophys Res Oceans. https://doi.org/10.1029/2019JC015960
Scargle J (1982) December. Studies in astronomical time series analysis. II. Statistical aspects of spectral analysis of unevenly spaced data. Astrophys J 263:835–853
Schnepf NR, Kuvshinov A, Sabaka T (2015) Can we probe the conductivity of the lithosphere and upper mantle using satellite tidal magnetic signals? Geophys Res Lett 42(9):3233–3239. https://doi.org/10.1002/2015GL063540
Schnepf NR, Manoj C, An C, Sugioka H, Toh H (2016) Time–frequency characteristics of tsunami magnetic signals from four pacific ocean events. In: Global tsunami science: Past and future, volume I, pp. 3935–3953. Springer
Schnepf NR, Manoj C, Kuvshinov A, Toh H, Maus S (2014) Tidal signals in ocean-bottom magnetic measurements of the Northwestern Pacific: observation versus prediction. Geophys J Int 198(2):1096–1110. https://doi.org/10.1093/gji/ggu190
Schnepf NR, Nair M, Maute A, Pedatella NM, Kuvshinov A, Richmond AD (2018) A comparison of model-based ionospheric and ocean tidal magnetic signals with observatory data. Geophys Res Lett 45(15):7257–7267. https://doi.org/10.1029/2018GL078487
Schureman P (1958) Manual of harmonic analysis and prediction of tides (Vol. 4). US Government Printing Office
Sulzbach R, Dobslaw H, Thomas M (2021) High-resolution numerical modelling of barotropic global ocean tides for satellite gravimetry. J Geophys Res Oceans 126(5):709e2020JC017
Thébault E, Finlay CC, Beggan CD, Alken P, Aubert J, Barrois O, Zvereva T (2015) International geomagnetic reference field: the 12th generation. Earth Planets Space 67(1):79. https://doi.org/10.1186/s40623-015-0228-9
Thomson RE, Emery WJ (2014) Data analysis methods in physical oceanography. Newnes
Toh H, Satake K, Hamano Y, Fujii Y, Goto T (2011) Tsunami signals from the 2006 and 2007 kuril earthquakes detected at a seafloor geomagnetic observatory. J Geophys Res Solid Earth 116:B2. https://doi.org/10.1029/2010JB007873
Tyler RH, Maus S (2003) Satellite observations of magnetic fields due to ocean tidal flow. Science 299(5604):239–241
VanderPlas JT (2018) Understanding the lomb–scargle periodogram. Astrophys J Supple Ser 236(1):16. https://doi.org/10.3847/1538-4365/aab766
Velímský J, Grayver A, Kuvshinov A, Šachl L (2018) On the modelling of *m2* tidal magnetic signatures: effects of physical approximations and numerical resolution. Earth Planets Space 70(1):192. https://doi.org/10.1186/s40623-018-0967-5
Virtanen P, Gommers R, Oliphant TE, Haberland M, Reddy T, Cournapeau D, SciPy 1.0 Contributors (2020) SciPy 1.0: fundamental algorithms for scientific computing in Python. Nat Methods 17:261–272. https://doi.org/10.1038/s41592-019-0686-2
Vivier F, Maier-Reimer E, Tyler RH (2004) Simulations of magnetic fields generated by the antarctic circumpolar current at satellite altitude: can geomagnetic measurements be used to monitor the flow? Geophys Res Lett 31:10. https://doi.org/10.1029/2004GL019804
Woolf HM (1968) On the computation of solar elevation angles and the determination of sunrise and sunset times. National Aeronautics and Space Administration
Young F, Gerrard H, Jevons W (1920) XIII. On electrical disturbances due to tides and waves. Lond Edinb Dublin Philos Mag J Sci 40(235):149–159. https://doi.org/10.1080/14786440708636105

Publisher's Note